Mechanotransduction and hyperpolarization-activated currents contribute to spontaneous activity in mouse vestibular ganglion neurons

Geoffrey C. Horwitz,[1,2,3] Jessica R. Risner-Janiczek,[3] and Jeffrey R. Holt[1,2]

[1]Department of Otolaryngology and [2]F.M. Kirby Neurobiology Center, Boston Children's Hospital and Harvard Medical School, Boston, MA 02115
[3]Department of Neuroscience and Otolaryngology, University of Virginia School of Medicine, Charlottesville, VA 22908

The hyperpolarization-activated, cyclic nucleotide–sensitive current, I_h, is present in vestibular hair cells and vestibular ganglion neurons, and is required for normal balance function. We sought to identify the molecular correlates and functional relevance of I_h in vestibular ganglion neurons. I_h is carried by channels consisting of homo- or heteromeric assemblies of four protein subunits from the *Hcn* gene family. The relative expression of *Hcn1–4* mRNA was examined using a quantitative reverse transcription PCR (RT-PCR) screen. *Hcn2* was the most highly expressed subunit in vestibular neuron cell bodies. Immunolocalization of HCN2 revealed robust expression in cell bodies of all vestibular ganglion neurons. To characterize I_h in vestibular neuron cell bodies and at hair cell–afferent synapses, we developed an intact, ex vivo preparation. We found robust physiological expression of I_h in 89% of cell bodies and 100% of calyx terminals. I_h was significantly larger in calyx terminals than in cell bodies; however, other biophysical characteristics were similar. I_h was absent in calyces lacking *Hcn1* and *Hcn2*, but small I_h was still present in cell bodies, which suggests expression of an additional subunit, perhaps *Hcn4*. To determine the contributions of hair cell mechanotransduction and I_h to the firing patterns of calyx terminals, we recorded action potentials in current-clamp mode. Mechanotransduction currents were modulated by hair bundle defection and application of calcium chelators to disrupt tip links. I_h activity was modulated using ZD7288 and cAMP. We found that both hair cell transduction and I_h contribute to the rate and regularity of spontaneous action potentials in the vestibular afferent neurons. We propose that modulation of I_h in vestibular ganglion neurons may provide a mechanism for modulation of spontaneous activity in the vestibular periphery.

INTRODUCTION

Normal vestibular function requires sensitive translation of physical movement into electrical signals and precise transmission from peripheral sensory organs to central processing areas. Vestibular information is used to drive postural reflexes, vestibular ocular reflexes that stabilize visual images on the retina, and for conscious perception of head movement. Vestibular transduction is initiated by cation influx through mechanosensitive ion channels located at the apical pole of vestibular hair cells. Mechanotransduction currents evoke graded receptor potentials, which modulate voltage-gated calcium channel activity and the release of glutamate at the hair cell basal pole. The graded receptor potentials are encoded postsynaptically into trains of action potentials that arise from the activity of AMPA receptors and perhaps through local K^+ accumulation in the synaptic cleft (Lim et al., 2011). Vestibular afferent fibers have cell bodies that reside in the vestibular ganglion. They relay vestibular information to brainstem and cerebellar nuclei via a branch of the eighth cranial nerve. To precisely

encode velocity, acceleration, and frequency of head movements requires that vestibular neurons modulate the rate and regularity of their resting discharge activity (Goldberg, 2000; Eatock and Songer 2011).

Recent data suggests that spontaneous activity in vestibular neurons may involve intrinsic biophysical properties (Kalluri et al., 2010). We hypothesized that a portion of the spontaneous activity is initiated in calyx terminals, unique postsynaptic structures that engulf the presynaptic cell bodies of type I hair cells. Despite considerable interest in calyx function, progress has been limited due to a lack of tractable experimental paradigms. Although reptilian systems and dissociated mammalian cells have been examined, data from intact mammalian systems are limited (Dulon et al., 2009; Songer and Eatock 2013). Therefore, we developed and characterized a semi-intact mouse preparation in which both whole-cell measurements of voltage-dependent currents and neuronal activity were recorded in a manner that preserved regional

information and the delicate hair cell–calyx morphological interaction. We used this preparation to investigate the contributions of mechanotransduction and I_h to spontaneous activity in dimorphic calyx terminals and in vestibular neuron cell bodies.

I_h has been investigated in vestibular calyces of gerbils (Meredith et al., 2012) and rats (Songer and Eatock, 2013) and the cell bodies of rat (Almanza et al., 2012) and mouse (Chabbert et al., 2001) vestibular ganglion neurons. However, the molecular identity, differences between the calyceal and cell body I_h, and the functional contributions of I_h to vestibular neuron activity have not been described. We used quantitative reverse transcription PCR (RT-PCR) and immunohistochemistry to show that *Hcn2* was the most highly expressed subunit, followed by *Hcn1* and *Hcn4*. I_h was larger in calyx terminals than in the cell bodies, which suggests up-regulation of channel density in calyx terminals. Our experimental paradigm facilitated identification of the molecular identity of I_h through recordings of *Hcn*-deficient mice. We show that calyx I_h is carried primarily by HCN2 and to a lesser extent by HCN1. In neuronal cell bodies I_h is carried by HCN1, -2, and -4. We characterized spontaneous activity recorded from calyx terminals, and found that spontaneous activity persists in the absence of mechanotransduction. We also found that modulation of I_h through application of the HCN antagonist ZD7288 or the HCN modulator cAMP alters firing rate and regularity in calyx terminals.

MATERIALS AND METHODS

Animals
All animal protocols were approved by the Animal Care and Use Committee of the University of Virginia (protocol No. 3123) or by the Animal Research at Children's Hospital (ARCH) of Boston Children's Hospital (protocol No. 11-04-1959). Five mouse genotypes of both genders were used to conduct experiments. Swiss Webster mice (Hilltop Lab Animals Inc. and Taconic Farms) as well as B6129SF2/J mice (The Jackson Laboratory) were used as control mice. Analysis of voltage-dependent currents, including, I_h and whole-cell capacitance values recorded from vestibular ganglion neurons, indicated no statistical differences between wild-type strains. Therefore, data from wild-type control mice were pooled for analysis. $Hcn1^{-/-}$ mice (B6;129-$Hcn1^{tm2Kndl}$/J) were generated as described previously (Nolan et al., 2003) and were obtained from The Jackson Laboratory (stock No. 005034). To preserve colonies and generate new breeders, $Hcn1^{-/-}$ mice were crossed with wild-type B6129SF1/J (stock No. 101043) mice from The Jackson Laboratory. $Hcn1^{+/-}$ mice were then crossed to generate new $Hcn1^{-/-}$ breeders. $Hcn1^{-/-}$ pups were generated from homozygous pairs of $Hcn1^{-/-}$ breeders. $Hcn2^{+/-}$ mice were obtained from Ludwig et al. (2003), which were generated on a C57BL/6 background. $Hcn2^{-/-}$ pups were generated from $Hcn2^{+/-}$ breeder pairs. *Hcn1/2* double knockout mice were created from crosses of $Hcn1^{-/-}$ and $Hcn2^{+/-}$ mice. $Hcn1^{+/-}$; $Hcn2^{+/-}$ mice were created and crossed, which gave rise to $Hcn1/2^{-/-}$ mice. Birth rates approximately followed the expected Mendelian ratio (1/16) for *Hcn1/2* double knockout mice.

Tissue preparation
Vestibular ganglia were excised from mice ranging in age from postnatal day zero to six (P0–P6). This age range was selected because the cell bodies of ganglion neurons undergo myelination after P6. Mice were decapitated and superior vestibular ganglia were removed by severing the peripheral afferent fibers and the fiber tracts of the vestibular branch of the eighth cranial nerve. No enzymatic dissociation was used. The ganglia were gently teased apart to expose the central region and placed as explant cultures (sometimes along with the utricle) onto glass coverslips coated with Cell-Tak (354240; BD) and maintained in vitro overnight at 37°C to allow for recovery from the dissection process. Dissections and culture were performed in MEM (41090-036; Invitrogen) supplemented with 0.05 mg/ml ampicillin and 10 mM HEPES, pH 7.4.

Calyx terminals were accessed through excision of the utricle sensory epithelium. Utricles were harvested at P8–P12 as described previously (Holt et al., 1997). This age range was selected because dimorphic calyx terminals were not clearly visible before P7 and because hair cells lack Na$^+$ currents by this developmental time point (Géléoc et al., 2004). In brief, mouse pups were killed by rapid decapitation and the temporal bones were excised and bathed in MEM supplemented with 10 mM HEPES and 0.05 mg/ml ampicillin, pH 7.4. Links between hair bundles and the otolithic membrane were broken with a 5-min incubation in dissection solution that contained 0.1 mg/ml Protease XXIV (Sigma-Aldrich). The utricle sensory epithelium was gently dissected and mounted on a glass coverslip beneath a pair of thin glass fibers glued to the coverslip to stabilize the tissue in a flat position. Care was taken to preserve as much of the afferent fiber track as possible during the dissection process. No enzymatic dissociations were performed. Calyx recordings were obtained from acute preparations.

Quantitative RT-PCR
10 vestibular ganglia were excised from five B6129SF2/J mice at P8, rinsed in MEM, and placed in lysis buffer for RNA extraction. Total RNA was extracted and purified using the RNAqueous-4PCR kit and TURBO DNA-free (Ambion), which yielded 1.06 µg. The RNA concentration (21.1 ng/µl) was measured using an ND-1000 Spectrophotometer (Thermo Fisher Scientific) and RNA quality was confirmed (RIN > 8.0) using a bioanalyzer (Agilent Technologies). 40 ng of RNA was reverse transcribed using the iScript cDNA Synthesis kit (Bio-Rad Laboratories, Inc.) and a Mastercycler gradient (Eppendorf). cDNA was synthesized (5 min at 25°C, 30 min at 42°C, and 5 min at 85°C) and diluted into 100 µl of buffer.

Quantitative RT-PCR primers for each *Hcn* subunit were designed using PrimerQuest Software from Integrated DNA Technologies (Horwitz et al., 2011) and primer efficiency was confirmed using standard curves as described previously (Horwitz et al., 2010). Expression of the housekeeping gene ribosomal 29S was monitored as a loading control. Quantitative PCR (qPCR) reactions were performed with the MyiQ Single-Color Real-Time PCR Detection System (Bio-Rad Laboratories) using iQ SYBR Green Supermix (Bio-Rad Laboratories) and RT-PCR grade water (Ambion). For qPCR we used 5 µl of template cDNA and the following program: 95°C for 3 min, 40 cycles of 95°C for 15 s, 30 s at the annealing temperature, and 72°C for 25 s (fluorescence detection and data collection occurred during these cycles), followed by 95°C for 1 min, 55°C for 1 min, and finishing with 80 cycles at 10 s each (55°C for the first two cycles with an increase in temperature of 0.5°C with each subsequent cycle). The latter sequence allowed for the generation of a melt curve, which confirmed a single melt temperature for each *Hcn* primer pair. MyiQ Optical System Software 1.0 was used for analysis of qPCR data. The copy number per vestibular ganglia was estimated for

each *Hcn* subunit from standard curves as described previously (Horwitz et al., 2010). The qPCR results are presented as means (± SEM) for six technical replicates from 10 biological samples harvested from five mice.

Immunofluorescence

During the dissections for immunohistochemistry experiments, the bony labyrinth was opened to expose the utricle and the tissue was bathed in MEM containing 0.1 mg/ml protease XXIV (Sigma-Aldrich) for 5 min. The otolithic membrane was removed and the vestibular ganglia and utricle were excised with connections still intact and placed as explant cultures onto glass coverslips coated with Cell-Tak. The co-cultures were fixed in 4% formaldehyde at room temperature (22–24°C) for 20 min. After three 5-min washes in 0.1 M PBS, the tissue was treated with 0.5% Triton X-100 for 30 min and then rinsed again in 0.1 M PBS (three times for 5 min). The tissue was incubated in a blocking solution that contained 3% normal goat or donkey serum and 3% bovine serum albumin in 0.1 M PBS at 4°C for 1 h. The primary antibody was applied and incubated overnight at 4°C and the secondary antibody was then applied for 1 h at 4°C. Before and after secondary antibody addition, the tissue was washed with 0.1 M PBS four times for 10 min. For control experiments, the primary antibody was omitted. The tissue was mounted on glass slides and imaged with a confocal microscope (LSM510; Carl Zeiss). For HCN1, the primary antibody was a goat polyclonal directed against the C terminus (sc-19706, 1:50 dilution; Santa Cruz Biotechnology, Inc.). For HCN2 and HCN4, the primary antibody was a rabbit polyclonal directed against the N terminus (APC-030, 1:100 dilution; Alomone Labs). The specificity of the HCN1 and HCN2 antibodies was confirmed through the use of knockout mice. The secondary antibodies, which varied depending on the primary antibody, were Alexa Fluor 488, 546, and 633 (1:200; Molecular Probes) and Cy5 (1:200; Jackson ImmunoResearch Laboratories, Inc.). Confocal images were also obtained of calyx terminals filled with Lucifer yellow. In this case, after fixation, samples were washed and immediately counterstained with Alexa Fluor Phalloidin (Invitrogen). Samples were imaged using a 63× objective lens on a confocal microscope (LSM510). Three-dimensional projection images were created using Imaris Scientific Software (Bitplane).

Electrophysiology

Vestibular ganglion neurons and calyx preparations were placed into a recording chamber and viewed with a microscope (Axioskop FS; Carl Zeiss) equipped with a 63× water-immersion objective lens and differential interference contrast optics. Recording pipettes were pulled from soda lime capillary glass (R-6; King Precision Glass) with resistances that ranged from 3.5 to 6.0 MΩ. The pipette tips were coated with ski wax to reduce pipette capacitance.

The whole-cell, tight-seal recording technique was used in both voltage-clamp and current-clamp modes. Cell bodies were held at −84 mV and calyces were held at −64 mV. Holding potentials were chosen to mimic experimentally measured resting potentials for calyx terminals and cell bodies. Data were acquired at room temperature using an amplifier (Axopatch 200B; Axon Instruments), filtered at 1 kHz with a low pass Bessel filter, digitized at 5 kHz with a 12-bit acquisition board, and acquired using pClamp 8.0 software (Axon Instruments).

Data were included in the analysis if they met the following criteria in voltage-clamp mode: expression of neuronal-type Na$^+$ currents and stable holding current of <100 pA at the holding potential. In current-clamp mode, the criteria for data analysis included stable resting potentials at hyperpolarized levels (−50 mV for cell bodies, −40 mV for calyx) as well as the ability to fire action potentials. Action potentials were characterized by voltage spikes with a clear upward inflection and peak voltages of ≥20 mV. If at any point during a recording the cell failed to meet these criteria, subsequent data were excluded from analysis. Many recordings lasted for >30 min and yielded variable rates and regularity at later stages in the recording. For a given cell, traces were selected for analysis that had the highest firing rate with the greatest regularity with the largest action potential peak to trough amplitude at the earliest time point during the recording.

Solutions

For vestibular ganglia electrophysiological recordings, cells were bathed in a standard extracellular solution that contained (in mM): 140 NaCl, 5 KCl, 1.3 CaCl$_2$, 1 MgCl$_2$, 10 HEPES, vitamins (1:100), and amino acids (1:50; Invitrogen) as in MEM. The solution was adjusted to pH 7.4 with NaOH and an osmolarity of 303 mosmol/kg. Recording pipettes were filled with an intracellular solution containing (in mM): 135 KCl, 2.5 Mg-ATP, 0.1 CaCl$_2$, 3.5 MgCl$_2$, 5 ethylene glycol-bis (β-aminoethyl ether)-*N,N,N',N'*-tetraacetic acid, and 10 HEPES, adjusted to pH 7.4 with KOH and an osmolarity of 277 mosmol/kg.

For calyx electrophysiology recordings, cells were bathed in standard artificial perilymph solution containing (in mM): 137 NaCl, 0.7 NaH$_2$PO$_4$, 5.8 KCl, 1.3 CaCl$_2$, 0.9 MgCl$_2$, 5.6 D-glucose, and 10 HEPES-NaOH, adjusted to pH 7.4 and 310 mosmol/kg. Vitamins (1:50), Glutamax (1:100), and amino acids (1:100) were added from concentrates (Invitrogen). Recording pipettes were filled with an intracellular solution containing (in mM): 132 KCl, 5 EGTA-KOH, 10 HEPES, 2.5 K$_2$ATP, 2.5 MgCl$_2$, 0.1 CaCl$_2$, 1.5 Lucifer yellow, and 1.5 glucose, pH 7.4. I_h currents were blocked/modulated in the calyx terminals using 100 µM ZD7288 (Tocris Bioscience) or 200 µM cAMP (Sigma-Aldrich).

ZD7288 is a well-established inhibitor of I_h in a variety of experimental paradigms (BoSmith et al., 1993). Drugs were included in the intracellular recording pipette to minimize off-target effects on remote sites that may be sensitive to extracellular drug delivery, including I_h and mechanotransduction channels in vestibular hair cells (Horwitz et al., 2010). Intracellular application of ZD7288 has been shown to be an effective modulator specific for I_h in spiral ganglion neurons (Kim and Holt, 2013), and we found no evidence of nonspecific effects of ZD7288 in vestibular ganglion neurons. Wu et al. (2012) reported that ZD7288 can block sodium currents in DRG neurons and in HEK cells transfected with NaV1.4. The lack of ZD7288 effect on sodium channels in vestibular ganglion neurons suggests that the vestibular neurons express a distinct population of sodium channels from the ZD7288-sensitive channels examined in the Wu et al. (2012) study. Indeed, the Shared Harvard Inner Ear Laboratory Database (SHIELD) reveals little expression of NaV1.4 (SHIELD accession no. Scn4a).

For the EGTA experiments, the sensory epithelia was dissected and immediately placed in extracellular solution in which Ca^{2+} was replaced by 5 mM EGTA. This incubation lasted 15 min, and has been shown previously to disrupt tip links (Assad et al., 1991; Marquis and Hudspeth, 1997). Previous reports indicate that there is no mechanotransduction current after EGTA incubation (Lelli et al., 2010). After the 15-min incubation, the sensory epithelium was returned to normal solutions containing 1.3 mM Ca^{2+} to ensure that synaptic machinery was functional. All experiments were completed within a 2-h window of EGTA treatment to minimize any potential recovery of the tip link complex.

Mechanical stimulation

Vestibular hair cell bundles were stimulated while recordings were made from the calyx in current-clamp mode. Stimulation was initiated by drawing the kinocilium into a pipette filled with extracellular solution and held in place with suction (Holt et al., 1997). Movement of the stimulus pipette was driven by a piezo-electric device that had a 10–90% rise time of 0.6 ms. Hair bundle deflections were monitored using a charge-coupled device camera

(C2400; Hamamatsu Photonics). Voltage steps were used to calibrate the motion of the stimulus probe ±2 µm relative to its rest position. Video images of the probe were recorded to confirm the absence of off-axis motion and to calibrate probe motion (spatial resolution of ∼4 nm). The position of the pipette and bundle were continuously monitored before, during, and after each recording using video microscopy to ensure that the stimulus pipette and the hair bundle moved in unison.

Analysis

Analysis was performed using Clampfit 8.1 software (Axon Instruments) and Origin 7.1 (OriginLab). All membrane potentials were adjusted for a 4-mV junction potential. Data are presented as means ± SEM, unless otherwise noted, and independent, two-sample t tests were used to determine statistical significance. To determine the activation range for HCN conductances, a Boltzmann equation of the following form was used:

$$G(V_m) = G_{min} + \frac{G_{max} - G_{min}}{1 + exp\left[-\left(V_m - V_{1/2}\right)/s\right]}.$$

The equation was fit to tail current scatter plots where G_{max} and G_{min} represent the maximum and minimum conductances, respectively. $V_{1/2}$ is the half-maximal voltage, and s represents the slope factor. G_{min} is corrected to zero.

RESULTS

Characterization of an ex vivo calyx recording paradigm

Vestibular sensory information is transmitted from hair cells to central vestibular pathways via vestibular afferent neurons. Here we present data from vestibular afferent neurons recorded from the cell bodies and calyx terminals (Fig. 1 A) within the intact sensory epithelium. Cell bodies were recorded from a semi-intact vestibular ganglion preparation as described previously (Risner and Holt, 2006). Calyx terminals were recorded from an ex vivo preparation in which hair cells and their synaptic terminals remained intact. Calyces were identified based on their distinct morphology. We focused on dimorphic calyces to maintain a uniform population. Unlike calyx-only or bouton-only terminals, dimorphic terminals vary discharge regularity based on their location (Baird et al., 1988; Goldberg et al., 1990). Dimorphic terminals, as depicted in Fig. 1 A (c), innervate both type I and type II vestibular hair cells. Dimorphic calyces were identified by the elongated neck region (Lysakowski et al., 2011). This morphological feature is unique to dimorphic calyx terminals and is easily identified near the hair cell apical surface (Fig. 1 B, arrows). The majority of calyx recordings were done with 1.5 mM Lucifer yellow in the recording pipette. After recording, a subset of dye-filled calyx preparations was fixed and imaged using confocal microscopy. Three-dimensional renderings allowed verification of the specificity of our recording paradigm and our calyx identification strategy (Fig. 1 C). After successful recordings, Lucifer yellow fluorescence was restricted to the calyx and along the afferent terminal field. No fluorescence was present in the innervated

type I hair cell. Diffusion of the dye allowed visualization of additional connected structures, including additional calyces and bouton endings (Fig. 1 C).

Robust inward Na$^+$ and outward K$^+$ currents were evoked by families of voltage steps that ranged between −104 mV and +96 mV in 10-mV increments from a holding potential of −64 mV (calyx terminals) or −84 mV (cell bodies). Holding potentials were selected based on resting potentials measured in current-clamp mode. Sodium and potassium currents, evident in both calyx terminals (Fig. 1 D) and cell bodies (Fig. 1 E), confirmed
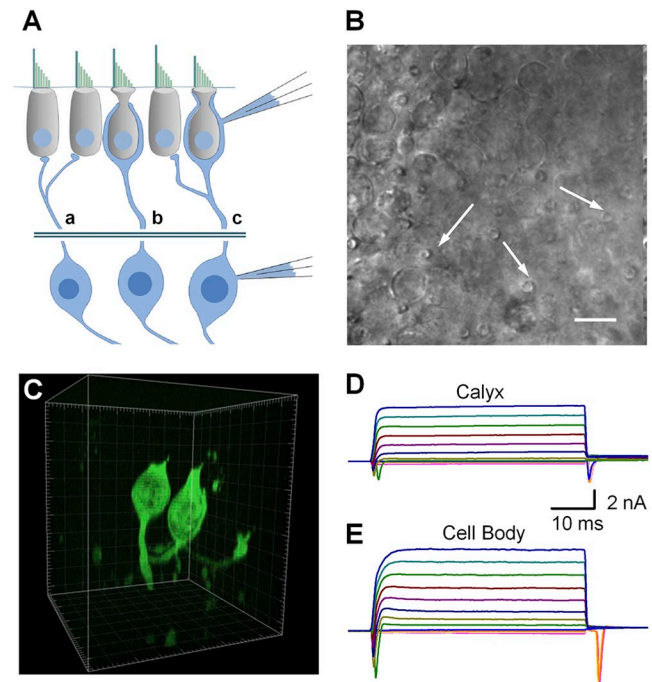

Figure 1. The semi-intact recording paradigm. (A) Illustration depicting the recording locations for vestibular ganglia neurons. Data were recorded from either calyx terminals of dimorphic afferent endings or from vestibular neuron cell bodies in isolated vestibular ganglion explants. The cross section through the sensory epithelia shows three types of afferent terminals: bouton (a), calyx only (b), and dimorphic (c). Dimorphic terminals innervate both type I and type II hair cells and were present in both central and peripheral zones. All recordings from terminals were from calyces of dimorphic endings. (B) Differential interference contrast image of the apical surface of the utricle preparation. Dimorphic calyces were identified by their restricted neck regions at the apical surface (arrows). (C) A subset of terminals was filled with Lucifer yellow introduced via recording pipettes. The tissue was fixed and imaged using confocal microscopy. A three-dimensional reconstruction shows the complex branching pattern of a typical dimorphic terminal that connects several calyces and bouton endings. Boxes are 10-µm cubes. (D and E) Representative families of voltage-dependent currents recorded from dimorphic calyx terminals (D) and vestibular neuron cell bodies (E). Inward Na$^+$ and outward K$^+$ currents were recorded in response to 50-ms voltage steps that ranged between −124 mV and 96 mV in 10-mV increments. Both Na$^+$ and K$^+$ currents were larger in the cell body than in calyx terminals. The scale bars apply to both current families.

that our pipettes were sealed onto vestibular ganglion neurons, as opposed to hair cells or glial cells.

Our intact, ex vivo preparation allowed the calyx data to be categorized based on location within the sensory epithelium. Calyx data are presented from either central or peripheral regions of the epithelium. The diagram in Fig. 2 A shows the utricle sensory epithelium split into central (dark gray) and peripheral (light gray) regions. Arrows indicate polarity of hair bundles while the dark gray line indicates the line of polarity reversal. Central and peripheral zones approximate striolar and extrastriolar regions; however, it was difficult to definitively identify the latter regions without the use of immunohistochemical markers. Data from the central zone were obtained from neurons located medial to the line of polarity reversal and separated from the periphery. Peripheral zone data were obtained from dimorph calyces within the first few rows of hair cells along the edge of the sensory epithelium and were encountered more frequently than central dimorphs.

Fig. 2 B shows an example of a compound calyx recording in which intracellular dye illuminates three connected calyces within a dimorphic ending. The mean number of calyces in a compound calyces in the central zone was similar to those in the peripheral zone (Fig. 2 C). The range was between one and five calyces per fill. Some dimorphic endings were complex, with a calyx terminal that engulfed two or more hair cells, but the majority was physically distinct, connected by branch points deep within the sensory epithelium. Boutons were too small and numerous to distinguish and count consistently. Physical measurement of the dye-filled calyces provided an estimation of calyx width at their widest points, measured from the outer surface to the inner surface, which juxtaposed the hair cell membrane. Peripheral calyces averaged 0.64 ± 0.04 µm ($n = 18$) while central calyces averaged 0.54 ± 0.04 µm ($n = 11$; Fig. 2 D). These results are similar to electron micrographs shown previously (Sousa et al., 2009).

Na$^+$ and K$^+$ current amplitudes were also analyzed as a function of epithelial location. K$^+$ currents were evoked in voltage-clamp mode using a family of steps between -104 mV and $+96$ mV at a holding potential of -64 mV. Fig. 2 (E and F) shows representative families of currents from peripheral and central calyces, respectively. Steady-state current–voltage (I-V) relationships showed little difference in the amplitudes of the K$^+$ currents measured in peripheral and central calyces (Fig. 2 G). Similarly, a comparison of peak inward Na$^+$ current amplitudes at steps between -54 mV and $+96$ mV from -64 mV showed little variation as a function of epithelial location (Fig. 2 H).

I_h in vestibular ganglion neurons

Recent studies of gerbils (Meredith et al., 2012) and rats (Almanza et al., 2012) identified and characterized

I_h in calyces and cell bodies of vestibular ganglion neurons, respectively. Here we extend this work to include vestibular neurons of wild-type mice and mice with genetic deletion of *Hcn1*, *Hcn2*, or both, combined with a pharmacological approach to identify the specific
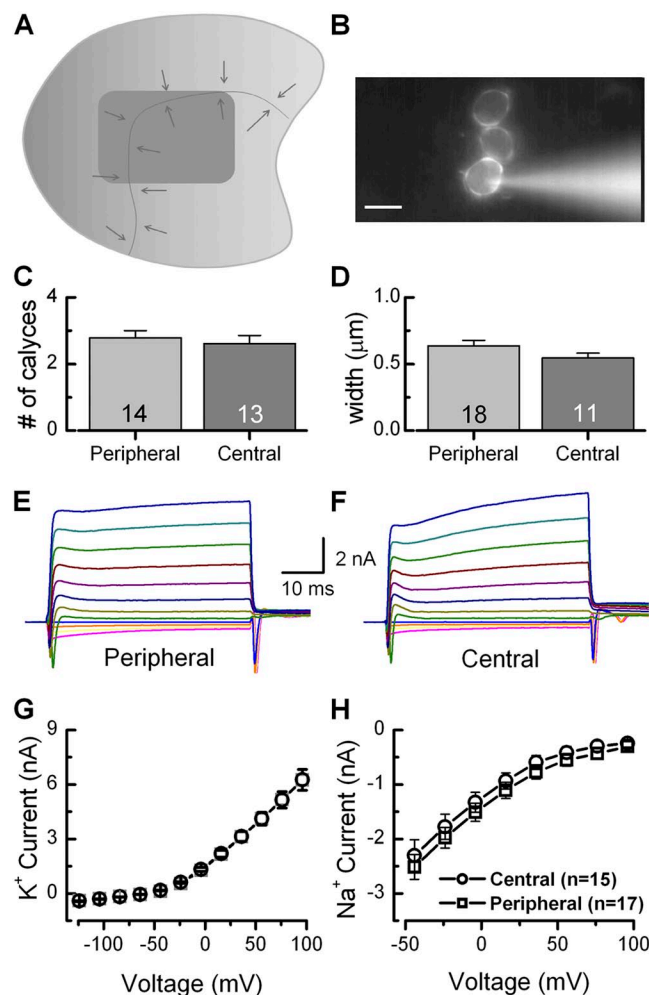

Figure 2. Characterization of the semi-intact mouse utricle preparation. (A) Illustration of utricle sensory epithelium showing the method of regional differentiation. Dimorphic terminals in the dark gray area were classified as central while dimorphic terminals in the light gray area were classified as peripheral. Arrows indicate bundle orientation around the line of polarity reversal. (B) Morphological characteristics were assayed through fluorescent imaging of Lucifer yellow–filled terminals. Bar, 10 µm. (C and D) We found no systematic differences in the number of calyces per terminal field (central: 2.6 ± 0.2, $n = 13$; peripheral: 2.8 ± 0.2; $n = 14$; C) or calyx width, measured from the external to the internal face juxtaposed the hair cell membrane (D) as a function of region. The number of samples is shown inside the bars for each condition. (E and F) Voltage steps between -124 mV and 96 mV in 10-mV increments elicited both inward Na$^+$ and outward K$^+$ currents. (G and H) I-V curves showed no differences in either steady-state K$^+$ or peak Na$^+$ currents as a function of location within the sensory epithelium. Space-clamp issues prevented further characterization of the large, fast K$^+$ and Na$^+$ currents but did not compromise characterization of the slower, smaller I_h in subsequent figures. Error bars indicate mean ± SEM.

Horwitz et al.   485

molecular correlates and functional relevance of I_h. Families of I_h were evoked by 2-s hyperpolarizing voltage steps in the cell bodies, peripheral dimorphic terminals, and central dimorphic terminals (Fig. 3, A–C). 90% ($n = 110$) of cell bodies and all calyx terminals ($n = 49$) displayed robust I_h in response to hyperpolarization. A previous study (Risner and Holt, 2006) classified vestibular neurons according to the current required to evoke action potentials: High threshold (HT) neurons required current injections of −176 pA on average, whereas low threshold (LT) required mean current injections of −43 pA. In this study, we found no difference in the properties of I_h between the two populations of neurons (P > 0.05). Therefore, I_h data from vestibular neuron cell bodies were pooled for subsequent analysis.

For a subset of calyx terminals ($n = 38$) and cell bodies ($n = 25$), we measured currents evoked by voltage steps that ranged between −144 mV and −64 mV in 10-mV increments from holding potentials of −84 mV (Fig. 3 A) or −64 mV (Fig. 3, B and C). The mean maximal current amplitude measured from cell bodies at −144 mV was −415 ± 35 pA ($n = 25$). Previous studies indicate that 100% of rat vestibular ganglion neuron cell bodies express inward currents that resemble I_h, with similar maximum current amplitudes: −400 ± 40 pA (Almanza et al., 2012). In calyx terminals, the mean amplitude measured at −144 mV was −902 ± 35 pA in the periphery ($n = 25$) and −934 ± 56 pA in the central regions ($n = 13$).

Because the direct measurement of current values can be contaminated by current through other ion channels or leakage, we opted to generate activation curves from tail currents measured at −74 mV, close to the reversal potential of potassium-selective inward rectifiers (Levin and Holt 2012) and negative to the activation range for voltage-dependent Na$^+$ and Ca^{2+} channels (Fig. 3, D–F).
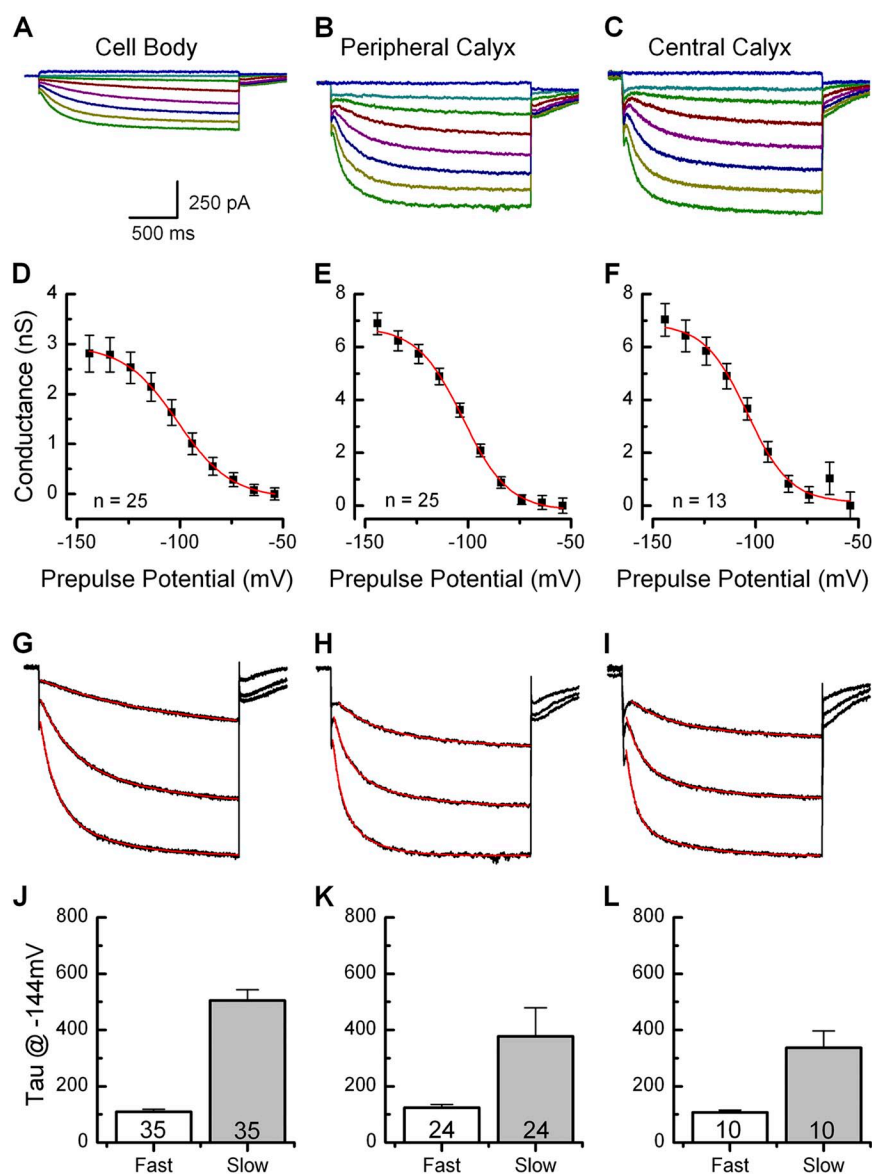

Figure 3. I_h in wild-type vestibular neuron cell bodies and calyx terminals. (A–C) I_h is activated in response to voltage steps between −144 and −64 mV in 10-mV increments in cell bodies (HP: −84 mV) and both peripheral and central dimorphic terminals (HP: −64 mV). (D–F) Activation curves generated from tail currents at −74 mV. Cell bodies displayed smaller maximum conductance than calyx terminals, but showed no differences in half-activation voltage or slope factor. (G–I) Traces recorded at −144, −124, and −104 mV from A, B, and C normalized for amplitude and fit with double exponential functions. (J–L) Fast and slow activation time constants were similar among the three populations. The number of samples is shown inside the bars for each condition. Error bars indicate mean ± SEM.

Conductance was calculated by dividing the tail currents, measured at the instant of the step, by the driving force, 30 mV. The conductance values were fit with a Boltzmann equation (see Materials and methods). G_h was taken as the difference between G_{Max} and G_{Min}. On average, the wild-type cell bodies had a maximal G_h of 3.5 ± 0.4 nS, a half-activation of −98.1 ± 1.2 mV, and a slope factor of 10.9 ± 0.5 mV ($n = 25$). Mean half-activation and slope factors were similar to those of rat vestibular ganglion cell bodies (Almanza et al., 2012). Peripheral dimorphic calyces had a mean maximal G_h of 7.1 ± 0.4 nS, a half-activation of −101.5 ± 1.0 mV, and a slope factor of 12.0 ± 0.5 mV ($n = 25$). Central dimorphic calyces had a mean maximal conductance of 7.4 ± 0.6 nS, a half-activation of −102.8 ± 1.3 mV, and a slope factor of 11.7 ± 0.7 mV ($n = 13$), which were not significantly different from measurements from peripheral dimorphic calyx I_h. Our data show a larger conductance and a more positive activation range than previously reported for gerbil calyx terminals (Meredith et al., 2012). Our biophysical measurements in calyx closely resemble those of cell bodies, whereas the previous gerbil calyx data displayed no open probability at potentials within the physiological range ($V_{1/2}$ of −123 mV and no channel activation positive to −100 mV). These differences may result from the short duration of the voltage steps used by Meredith et al. (2012), species differences, or age differences. We suggest that our semi-intact preparation provides an alternative method for studying calyx terminals and may produce values closer to those expected in vivo.

Interestingly, we noted that the maximal G_h and I_h values were significantly larger in calyx terminals than in the cell bodies. Whether this is a consequence of the difference in holding potential, differences in the age of the preparations, or of the up-regulation of HCN channel density in calyx terminals has not been determined. However, because the capacitance was similar between cell bodies (10–13 pF; Risner and Holt, 2006) and calyx terminals (13.6 ± 4.7 pF; $n = 46$), we favor the latter explanation. Regulation of HCN channel density has also been documented in other neuronal preparations (Magee, 1999).

Previously reported activation kinetics for both vestibular afferent cell bodies and calyx terminals were fit with single or double exponential functions. To characterize the activation kinetics of neuronal I_h, traces generated at −144 mV, −124 mV, and −104 mV were fit with double exponential functions (Fig. 3, G–I). Traces shown in G, H, and I are the same traces shown in A, B, and C but were normalized to the maximal amplitude to facilitate comparison of activation kinetics (Fig. 3). Activation kinetics of I_h were voltage-dependent, with steps to −144 mV activating more rapidly than steps to −104 mV in all three populations. Fast and slow time constants of activation were statistically similar across all

three populations (Fig. 3, J–L). Cell body I_h activated with a fast time constant of 109.4 ± 9.4 ms and a slow time constant of 504.5 ± 39.1 ms ($n = 35$). Peripheral dimorphic calyces activated with a fast time constant of 123.7 ± 11.0 ms and a slow time constant of 377.4 ± 102.0 ms ($n = 24$). Central dimorphic calyces activated with a fast time constant of 107.3 ± 7.1 ms and a slow time constant of 337.4 ± 59.1 ms ($n = 10$). Activation kinetics were slower than those reported previously in vestibular hair cells, which indicates contributions from subunits other than HCN1 (Ludwig et al., 1999; Santoro et al., 2000; Horwitz et al., 2011).

Molecular identification of vestibular afferent I_h

To determine the molecular identity of the channels responsible for the generation of I_h in mouse vestibular ganglion neurons, we examined the relative expression level of *Hcn1–4* transcripts using quantitative RT-PCR with the *Hcn*-specific primer sets validated in prior publications (Horwitz et al., 2010, 2011; Kim and Holt, 2013). Total RNA was extracted from 10 vestibular ganglia excised from five B6129SF2/J P8 mice and reverse transcribed into cDNA. We found *Hcn2* to be the most highly expressed subunit (Fig. 4 A). The expression ratio for *Hcn1–4* was 24:40:1:6, respectively.

To confirm that the detected mRNA transcripts were translated into HCN protein, expression was confirmed using immunohistochemistry. Antibodies specific to HCN1, HCN2, and HCN4 were used to localize HCN channels in postnatal vestibular ganglia. Vestibular neuron cell bodies were identified using anti–Neurofilament-200 (not depicted). Immunostaining of calyx membranes was examined previously (Horwitz et al., 2011). In cell bodies, we found robust staining for HCN1, HCN2, and HCN4 (Fig. 4, C–E) in wild-type neurons. Labeling was strongest around the membrane, which is consistent with the presence of functional ion channels. To quantify the expression level, we counted the number of HCN-positive neurons as a percentage of Neurofilament-200–positive neuronal cell bodies. HCN2 was expressed in 100% of neurons ($n = 983$), whereas HCN1 and HCN4 were expressed in 42% and 53% of Neurofilament-200–positive neurons ($n = 1,375$ and 438, respectively; Fig. 4 B). High HCN2 expression relative to HCN1 and HCN4 was consistent with our qPCR data.

To investigate the functional contributions of HCN subunits in vestibular ganglion neurons, we recorded I_h from wild-type mice (Fig. 5, A and B) and mice lacking *Hcn1*, *Hcn2*, or both (Fig. 5, C–H). In contrast with data from vestibular hair cells (Horwitz et al., 2011), I_h was present in *Hcn1*-deficient vestibular neuron cell bodies (Fig. 5 C) and in dimorphic calyx terminals (Fig. 5 D). We found robust I_h in 96% of cell bodies (Fig. 5 I, $n = 52$) and 100% of calyx terminals from *Hcn1*-deficient mice (Fig. 5 J, $n = 21$). However, we did note that loss of functional *Hcn1* expression caused a 50% reduction of

the maximum conductance to 1.6 ± 0.3 nS ($n = 11$, P < 0.01) in cell bodies and a 10% reduction to 6.3 ± 0.6 nS ($n = 20$) in dimorphic calyx terminals (Fig. 5, K and L). Activation of I_h in *Hcn1*-deficient mice resulted in a $V_{1/2}$ of -108.5 ± 1.4 mV ($n = 11$) in cell bodies and -109.8 ± 1.3 mV in dimorphic calyx terminals (Fig. 5, M and N). This reflects a significant (P < 0.001) negative shift in both populations: 10 mV in cell bodies and 8 mV in dimorphic calyces. I_h from *Hcn1*-deficient cell bodies and dimorphic calyx terminals activated more slowly (P < 0.001) than I_h in wild-type neurons. The mean fast time constant of activation was 440.5 ± 38.0 ms ($n = 13$) in cell bodies and 196.7 ± 9.3 ms ($n = 21$) in calyx terminals (Fig. 5, O and P). The slow time constant of activation remained unchanged in *Hcn1*-deficient mice. HCN1 expressed in heterologous cells yields currents with faster activation and more positive $V_{1/2}$ potentials relative to other HCN subunits (Santoro et al., 2000). As such, our results from *Hcn1*-deficient mice reflect the expected biophysical changes in currents carried by multiple HCN subunits after loss of HCN1.

I_h was also examined from cell bodies and dimorphic calyx terminals in *Hcn2*-deficient mice. We found that I_h persisted in 94% of *Hcn2*-deficient cell bodies (Fig. 5, D and I, $n = 33$) but only 62.5% of *Hcn2*-deficient calyx terminals (Fig. 5, F and J, $n = 16$). The maximum conductance was statistically unchanged in cell bodies at 4.0 ± 0.5 nS ($n = 23$); however, dimorphic calyx I_h was significantly reduced (P < 0.001) by 59% to 2.9 ± 0.6 nS ($n = 16$; Fig. 5, K and L). *Hcn2* activates more slowly and at more negative potentials than *Hcn1* (Ludwig et al., 1999), therefore we hypothesized that residual I_h from *Hcn2*-deficient mice would reflect loss of negatively activated, slower currents. $V_{1/2}$ was 3 mV more positive (-95.9 ± 1.8 mV, $n = 20$) in cell bodies and significantly (P < 0.001) more positive (-95.1 ± 0.9 mV, $n = 10$) in calyx terminals (Fig. 5, M and N). Activation kinetics were also significantly faster (P < 0.05) in the absence of *Hcn2*. The fast time constant of activation was 78.4 ± 4.9 ms ($n = 20$) in cell bodies and 65.0 ± 9.9 ms ($n = 6$) in dimorphic calyx terminals (Fig. 5, O and P).

Because both *Hcn1*- and *Hcn2*-deficient vestibular neurons displayed evidence of residual I_h, we next examined I_h in vestibular neurons of *Hcn1/2* doubly deficient mice. Small, slowly activating I_h was still evident in vestibular neurons of *Hcn1/2* double knockout mice (Fig. 5, G and I). The conductance was reduced to 1.7 ± 0.4 nS (Fig. 5 K), the voltage of half-activation was -113.2 ± 2.7 mV (a difference of -14 mV; Fig. 5 M), the fast activation time constant was 997.1 ± 87.6 ms, and the slow time constant was 1.8 ± 0.7 s (Fig. 5 O). Based on our molecular, immunohistochemical, and electrophysiological data, we suggest that *Hcn4* plays a minor role in the generation of the cell body I_h. As *Hcn4*-deficient mice were not available, we were unable to confirm this suggestion with direct measurements.

I_h was completely absent in all dimorphic calyx terminals tested (Fig. 5, H and J, $n = 17$). Fast inward rectifying potassium current remained. However, as the tail currents were measured at -74 mV (near the potassium equilibrium potential) it was clear that all I_h was eliminated. Collectively, these results indicate that I_h is carried by different subunits depending on the location in vestibular afferent neurons. We conclude that I_h is carried by HCN1 and HCN2 in mouse vestibular calyx terminals and by HCN1, HCN2, and perhaps HCN4 in neuronal cell bodies, which is consistent with rat data from Almanza et al. (2012), who reported immunolocalization of HCN1, -2, and -4 in the vestibular ganglia but only HCN1 and -2 in the sensory epithelium.
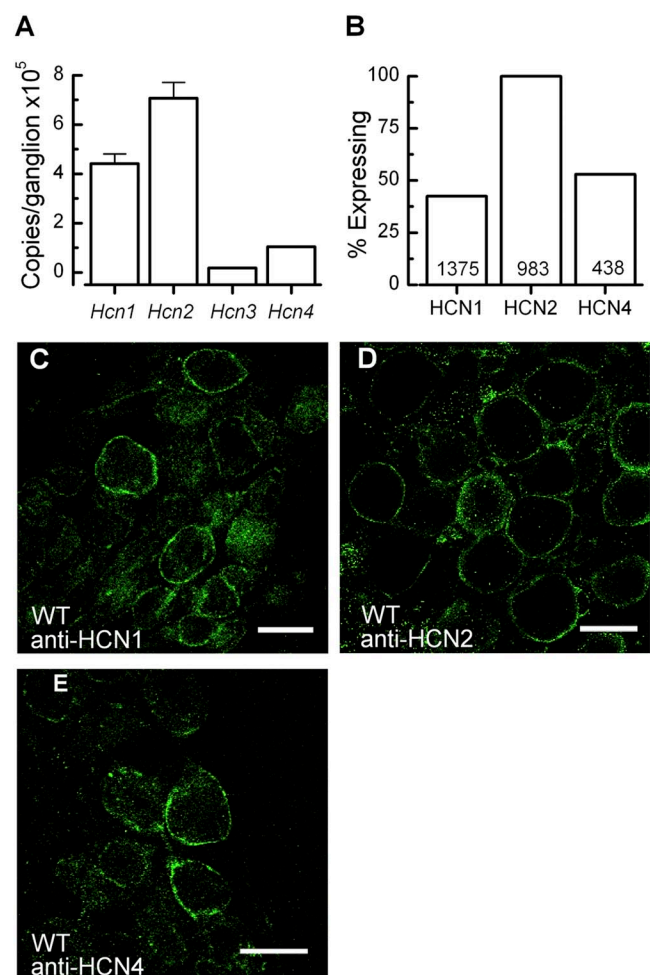

Figure 4. Expression of *Hcn* subunits in the vestibular neuron cell bodies. (A) Quantitative RT-PCR was used to estimate the mRNA expression level/vestibular ganglion for each of the four *Hcn* subunits from a pool of 10 vestibular ganglia at P8. Error bars represent SEM from six technical replicates. (B) The percentage of Neurofilament-200–positive vestibular neuron cell bodies that expressed HCN1, -2, or -4. The numbers of cells counted for each HCN subunit are shown at the bottom. (C–E) Representative immunolocalization images for HCN1 (C), HCN2 (D), and HCN4 (E) wild-type vestibular neuron cell bodies (P8). Images of these sorts were used to generate the counts shown in B. Bars, 20 µm.

Characterization of firing properties in calyx terminals

In addition to whole-cell recordings of voltage-dependent currents, our intact ex vivo preparation allowed us to record from calyx terminals in current-clamp mode while preserving utricular regional information and dimorphic structure. Vestibular neurons have been classified as either regular or irregular based on their spontaneous firing patterns (Baird et al., 1988; Goldberg et al., 1990). Regularly firing neurons originate predominately from peripheral or extrastriolar regions, whereas irregularly firing neurons originate primarily from central or striolar regions (Goldberg and Fernández, 1977; Goldberg et al., 1990). When we recorded from dimorphic calyx terminals we found robust spontaneous action potential firing. Calyces were identified as spontaneous if they reproducibly fired action potentials during a 20-s recording. The mean and standard deviation of the interspike interval were calculated for every 20-s trace. Standard deviation was divided by the mean to estimate the coefficient of variation (CV). Recordings were then classified as either regular (Fig. 6 A)

based on CV ≤ 0.25 or irregular (Fig. 6 B, CV > 0.25). Consistent with previous studies (Baird et al., 1988), we observed a continuous distribution. Firing properties varied with location of dimorphic terminals within the utricle. Peripheral calyx terminals fired spontaneous action potentials more often than centrally located calyx terminals (Fig. 6 C). 61% of peripheral terminals ($n = 23$) fired spontaneous action potentials versus 38% of centrally located terminals ($n = 13$). Peripheral dimorphic terminals that were spontaneously active also displayed a higher firing rate (Fig. 6 D), which is consistent with a recent report from rat calyx terminals (Songer and Eatock 2013). Peripheral dimorphic calyces fired at 11.3 ± 1.2 spikes/s ($n = 14$) while centrally located dimorphic calyces fired at 5.5 ± 1.9 spikes/s (P < 0.05, $n = 5$). Irregular neurons may correspond to high threshold neurons (Risner and Holt, 2006), and this may contribute to a greater population of quiescent or slowly spiking terminals. Alternatively, as centrally located dimorphs innervate hair cells with larger, more delicate bundles, it is also possible that some of the difference
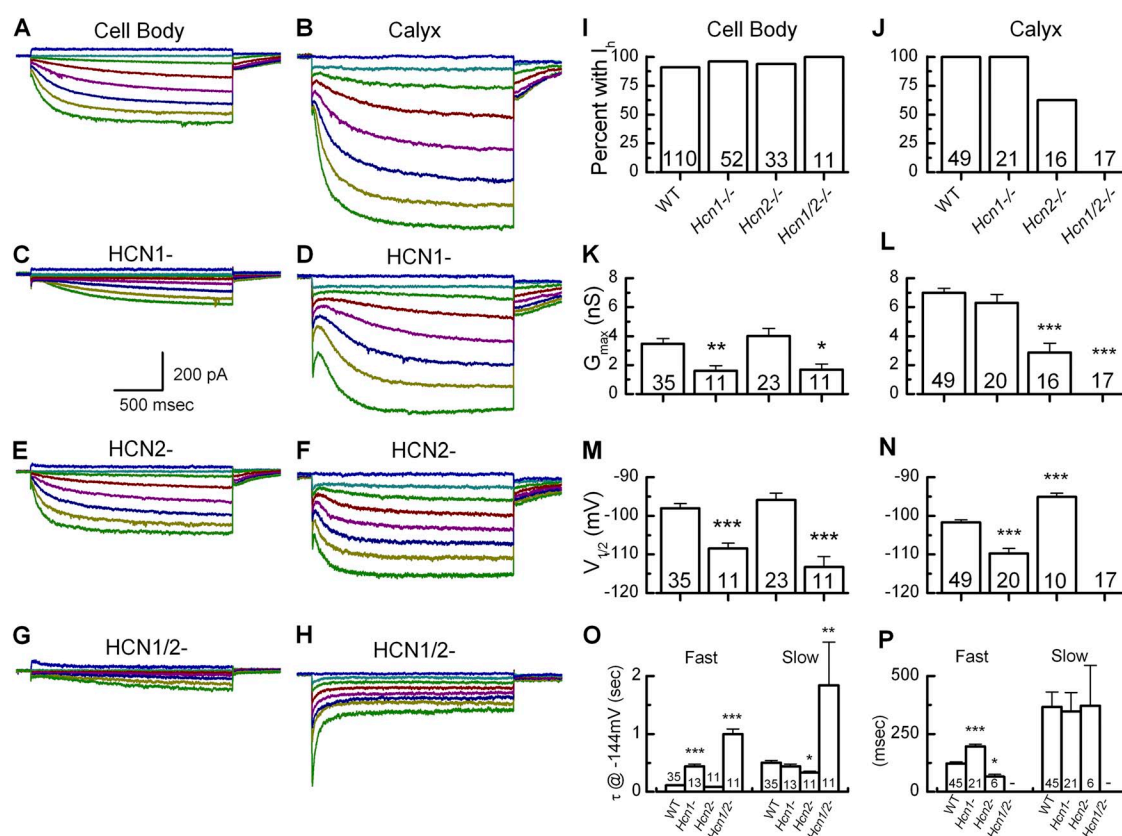

Figure 5. I_h in cell bodies and dimorphic terminals of *Hcn*-deficient mice. Representative traces of I_h generated from voltage steps between −144 and −64 mV in 10-mV increments recorded from cell bodies (A, C, E, and G) or dimorphic terminals (B, D, F, and H). (A and B) Representative traces from wild-type mice. (C–H) Representative traces from *Hcn1* (C and D)-, *Hcn2* (E and F)-, or *Hcn1/2* (G and H)-deficient neurons. I_h was completely absent in *Hcn1/2* calyx terminals (H) but remained in cell bodies (G). The residual current in H is likely the fast potassium inward rectifier I_{K1}. (I–P) Biophysical properties from wild-type and *Hcn1*-, *Hcn2*-, and *Hcn1/2*-deficient neuron cell bodies (I, K, M, and O) and calyx terminals (J, L, N, and P). Asterisks indicate statistical significance relative to wild-type: *, P < 0.05; **, P < 0.01; ***, P < 0.001. The number of samples is shown inside the bars for each condition. Error bars indicate mean ± SEM.

is due to damage associated with excision of the sensory epithelium. We also recorded regional differences in regularity. Half of the peripheral dimorphic calyces fired irregularly. In contrast, all of the central dimorphic calyces fired irregularly, with coefficients of variation at or above 0.36 (Fig. 6, E and F).

Origin of spontaneous activity

To investigate the origin of spontaneous activity in calyx terminals, we recorded from >160 dimorphic calyces. Previous work in zebrafish lateral line organs indicated that resting spiking in afferent neurons depends on neurotransmission from presynaptic hair cells (Trapani and Nicolson 2011). Due to resting tension in the mechanotransduction complex, 10–20% of mechanotransduction channels are open and allow tonic cation influx. This depolarizes hair cells into the range of calcium channel activation, which in turn promotes tonic neurotransmitter release (Hudspeth, 1989). Therefore, we hypothesized that spontaneous activity in mouse calyx terminals may also be influenced by current through mechanotransduction channels open at rest. To test this hypothesis we recorded from dimorphic calyx terminals in the presence or absence of hair bundle stimulation (Fig. 7 A). In the absence of mechanical stimulation the mean spontaneous firing rate was 9.3 ± 4.2 spikes/s ($n = 6$), similar to values reported in Fig. 6 D. When the bundle was deflected in the positive direction, the mean firing rate increased to 16.5 ± 5.1 spikes/s (Fig. 7 B). When the bundle was deflected in the negative direction, the mean firing rate dropped to 8.0 ± 3.7 spikes/s. The change in spike rate between positive and negative bundle positions was highly significant (Fig. 7 C; $P = 4.2 \times 10^{-4}$), which indicates that hair bundle deflection modulates the firing rate in dimorphic calyx terminals. Interestingly, negative bundle deflections did not reduce the firing rate to zero. As shown previously, most dimorphic terminals are connected to at least two additional calyces as well as several bouton endings. Therefore, in a dimorphic terminal field that innervates multiple hair cells, the nonzero firing rates after negative deflection of a single bundle may reflect the activity of other hair bundles that remained in the rest position.

To assay the contribution of resting mechanotransduction to the firing rate across an entire dimorphic terminal field, we disrupted tip links in the entire utricle epithelium with a 15-min incubation in 5 mM EGTA. At the end of the EGTA treatment, the sensory epithelia were returned to standard solutions containing 1.3 mM Ca^{2+}. This EGTA protocol has been shown to eliminate mechanotransduction currents for up to 2 h (Lelli et al., 2010). The following recordings were completed within 2 h of EGTA treatment, before the recovery of transduction. Surprisingly, we found only a slight decrease in the number of spontaneously active cells, from 61% to 44% (Fig. 7 D). However, for those calyx terminals that were

active, there was a significant ($P < 0.01$) decrease in the spontaneous firing rate after EGTA treatment: 3.5 ± 2.1 spikes/s ($n = 4$; Fig. 7 E). These results indicate that mechanotransduction currents active at rest contribute to spontaneous firing in dimorphic terminals.

Importantly, a significant portion of spontaneous activity remained after negative bundle deflections and after treatment with EGTA. Prior evidence supports a postsynaptic mechanism as a possible origin of spontaneous activity in some afferent neuron populations (Hirvonen et al., 2005). Therefore, we wondered whether I_h in dimorphic calyx terminals may also contribute to spontaneous firing in vestibular afferent neurons. To test this possibility, we included ZD7288, cAMP, or both in
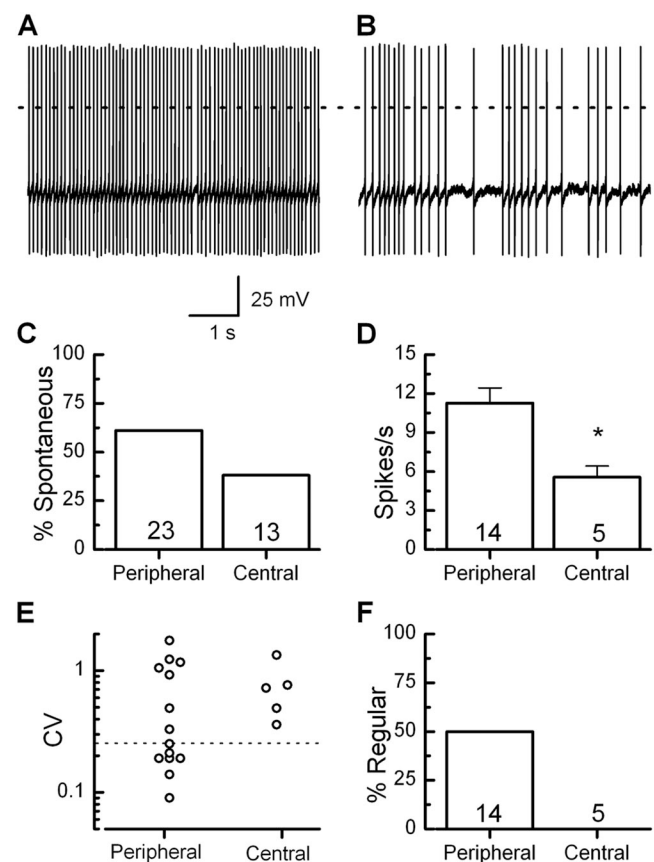

Figure 6. Regional variability in spontaneous firing properties of dimorphic terminals. (A and B) Representative examples of dimorphic terminals that fired with regular (A) and irregular (B) patterns. (C) Percentage of dimorphic terminals that were spontaneously active at rest as a function of region. (D) Firing rate was calculated for calyx terminals with spontaneous activity. The firing rate was significantly lower in the central region than in the periphery. Error bars indicate mean ± SEM. (E and F) Peripheral dimorphic terminals fired with greater regularity than centrally located dimorphic terminals. The CV was calculated by dividing the standard deviation of the interspike interval by the mean. Regular is indicated by the broken line at <0.25. *, P < 0.05. The number of samples is shown inside the bars for each condition.

the recording pipette to modulate I_h in calyx terminals without affecting hair cell channels.

As expected, introduction of 100 µM ZD7288 in the recording pipette blocked I_h completely (Fig. 8, B and D), whereas 200 µM cAMP enhanced the activity of I_h at rest (Fig. 8 C). Intracellular application of cAMP did not alter the maximal amplitude of G_h (Fig. 8 D), but resulted in a statistically significant shift ($P < 0.001$; +6 mV) of the half-activation voltage to -95.0 ± 1.2 mV (Fig. 8 E). Intracellular cAMP also increased the speed of activation, decreasing the fast time constant by 33% to 82.3 ± 8.2 ms and the slow time constant by 37% to 230.6 ± 44.9 ms (Fig. 8 F). Because cyclic nucleotides have been shown to interact with KCNQ4 channels in the inner ear (Jagger and Ashmore 1999; Chambard and Ashmore 2005; Pattnaik and Hughes 2012) and KCNQ4 has been localized in calyx membranes (Hurley et al., 2006), we examined steady-state I-V curves for outward K^+ currents in control and cAMP-treated dimorphic terminals. We detected no differences between the two populations (Fig. 8 G), which suggests that in our experiments, the cAMP effect was specific for I_h.

To investigate I_h contributions to the firing properties of dimorphic calyx terminals, we recorded calyx activity in current-clamp mode while modulating I_h with ZD7288, cAMP (Fig. 9, A and B), or both. We found that blocking I_h with ZD7288 in the recording pipette resulted in fewer spontaneously active calyx terminals, decreasing from 61% to 23% (Fig. 9 C). Of the spontaneously active calyx terminals, there was no difference in spike rate between control and ZD788-treated calyces. In contrast, modulation of I_h with cAMP showed little effect on the number of spontaneously active calyces (56% spontaneous) but increased the firing rate by 44% to 16.1 ± 1.3 spikes/s (Fig. 9 D). This increase was statistically significant ($P < 0.05$) and was similar to the increase seen after stimulating the vestibular hair cell bundle. Because cAMP shifts the activation curve of I_h toward positive potentials, a greater fraction of G_h was active at rest. G_h at V_{rest} was estimated by measuring the conductance from the activation curve at the resting potential for each calyx. A plot of G_h at V_{rest} versus firing rate revealed a strong correlation ($P < 0.01$; Fig. 9 F), which suggests that the effect of cyclic nucleotides on the firing rate of dimorphic terminals is through modulation of HCN channel activity. Interestingly, we also found that calyx I_h contributes to spike regularity. Loss of I_h in ZD7288-treated cells resulted in highly irregular firing with a high mean CV of 1.1 ± 0.1 (Fig. 9 E), whereas shifting the activation range of I_h with cAMP resulted in a sharp increase in regularity and a corresponding decrease in the CV to 0.09 ± 0.01 (Fig. 9 E). This change in regularity from cyclic nucleotides was through modulation of I_h, as it could be blocked through inhibition of I_h with ZD7288 even in the presence of cAMP (Fig. 9 E). As expected, a plot of G_h at V_{rest} versus CV demonstrated

a strong correlation ($P < 0.01$; Fig. 9 G), which suggests that I_h contributes to spike regularity.

To identify the biophysical changes associated with this change in firing regularity, we generated spikes in current-clamp mode in both wild-type and ZD7288-treated calyx terminals by hyperpolarizing to ~ -100 mV and then returning to rest. No additional current was injected to evoke an action potential. As a result of HCN channels open at hyperpolarized potentials, the latency to the peak of the spike was much shorter in the
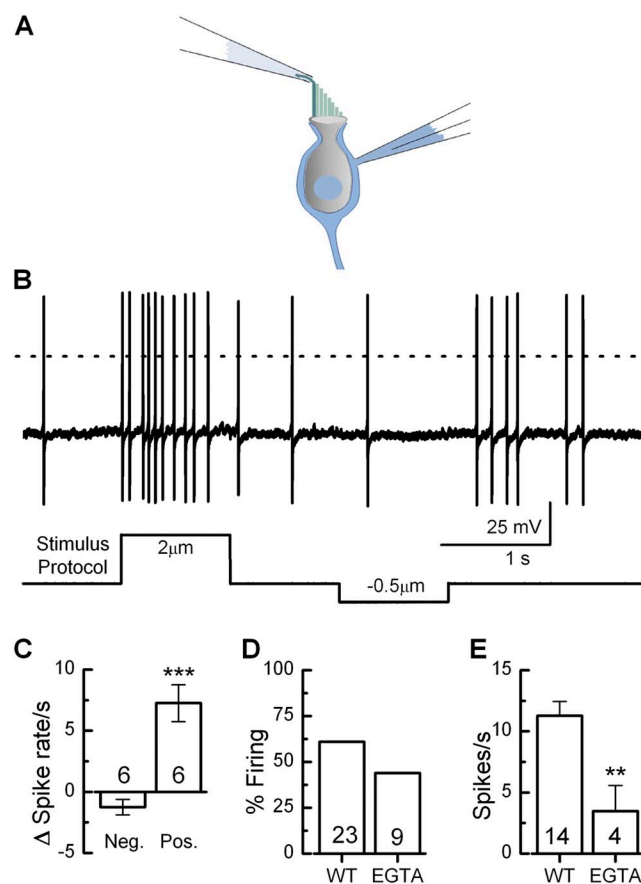

Figure 7. Hair cell mechanotransduction contributes to spontaneous activity in dimorphic terminals. (A) A schematic diagram illustrating a slice through the sensory epithelium and our stimulation/recording paradigm. Data were recorded from calyx terminals while stimulating the hair bundle of the innervated type I hair cell. Individual hair bundles were deflected with a stiff probe coupled to the kinocilium. (B) Representative current-clamp trace showing modulation of the firing rate in a dimorphic calyx terminal using the hair bundle deflection protocol shown below. (C) Change in spike rate, relative to the spike rate at rest, plotted as a function of bundle deflection (toward the kinocilium is positive). Positive deflections increased the firing rate, whereas negative deflections decreased the firing rate. ***, $P < 0.001$. (D and E) Firing properties were also examined after treatment with EGTA to eliminate mechanotransduction. The percentage of spontaneously active calyx terminals was slightly reduced (D), but the firing rate was significantly lower in the absence of mechanotransduction (E). **, $P < 0.01$. The number of samples is shown inside the bars for each condition. Error bars indicate mean ± SEM.

majority of wild-type calyx terminals (Fig. 10 A). Maximum amplitudes were similar, as ZD7288 did not alter the properties of Na$^+$ channels (Fig. 10 B). Finally, repolarization was slower in many of the ZD7288-treated calyx terminals (Fig. 10 C), which suggests that I_h functions to speed the repolarization phase at the end of an action potential.

DISCUSSION

The preparation
Although considerable progress has been made using dissociated vestibular preparations from various species (Hurley et al., 2006; Rennie and Streeter 2006), there remains a dearth of physiological information from intact calyx terminals in vestibular organs of the mouse, a model system amenable to genetic manipulation. Here we characterized a semi-intact utricle preparation that allowed for reliable, stable recording from dimorphic calyx terminals in peripheral and central regions of wild-type and *Hcn*-deficient mice. Using terminals filled with fluorescent dye and confocal microscopy, we imaged the complex morphology of vestibular afferent terminal fields, confirmed the innervation patterns with calyx and bouton connections to adjacent hair cells, and verified structural integrity of the terminals. We recorded robust voltage-dependent Na$^+$, K$^+$, and HCN currents, and, in current clamp mode, recorded large-amplitude action potentials evoked by hair bundle deflections, as well as spontaneous activity recorded in the absence of stimulation. Spontaneous activity in vestibular afferent

neurons is a critical property for normal vestibular function. The firing rate can be modulated in either direction by hair bundle deflections of opposite polarity. Furthermore, spontaneous activity places the afferent fiber within a more sensitive range of the stimulus–response relation.

Our data reveal that spontaneous action potentials are initiated within calyx terminals of mouse vestibular end organs. Previous reports from excised vestibular neuron cell bodies (Risner and Holt, 2006; Kalluri et al., 2010) and dissociated calyx preparations (Meredith et al., 2012) showed little spontaneous activity. Therefore, we conclude that the initiation of spontaneous activity in vestibular neurons depends on the delicate physical interaction between vestibular hair cells and calyces in dimorphic terminals. Moreover, our data demonstrate that the location of dimorphic terminals within the intact epithelium is correlated with the regularity of spontaneous activity, which is consistent with prior classification (Baird et al., 1988; Goldberg et al., 1990). We propose that firing pattern regularity in vestibular afferent neurons originates, in part, within dimorphic terminals themselves.

Regional differences in dimorphic terminals
We find that dimorphic terminals have distinct discharge properties depending on their location within the sensory epithelium. Previous reports have indicated that centrally located afferent fibers fire irregularly, whereas peripherally located fibers fire regularly (Goldberg 2000). Our results corroborate these findings, therefore we
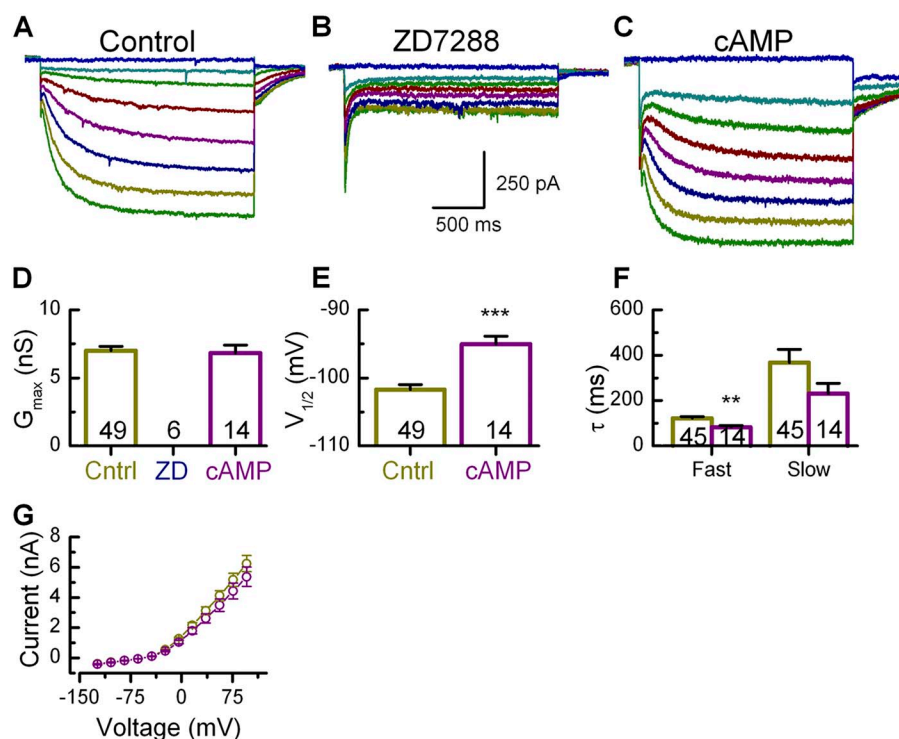

Figure 8. Calyx I_h was modulated by ZD7288 and cAMP. (A) Representative traces from a wild-type dimorphic terminal in response to voltage steps between -144 mV and -64 mV in 10-mV steps. (B) I_h was blocked by inclusion of 100 µM ZD7288 in the recording pipette. (C) Representative I_h after the addition of 200 µM cAMP in the pipette. (D) G_{max} and $V_{1/2}$ were estimated from activation curves generated as described for Fig. 3 (D–F). The conductance was completely blocked by ZD7288 but unaffected by cAMP. (E) cAMP shifted the voltage of half maximal activation in the positive direction. (F) cAMP increased the activation speed, shown here as a decrease in both fast and slow time constants. The number of samples is shown inside the bars for each condition. **, P < 0.01; ***, P < 0.001. Error bars indicate mean ± SEM. (G) Steady-state I-V plots from calyx terminals with cAMP did not reveal any change in voltage-dependent K$^+$ currents.

have retained this classification scheme. We hypothesize that differences in intrinsic membrane properties may contribute to these regional differences. Surprisingly, we found no overt differences in K^+ or Na^+ currents between central and peripheral dimorphic terminals. Calyx terminals contain two populations of K^+ channels: a rapidly activating, rapidly inactivating current sensitive to 4-AP and a slowly activating current sensitive to TEA (Dhawan et al., 2010). It is possible that these distinct potassium conductances may contribute to subtle differences in central versus peripheral dimorphs that were not revealed by analysis of steady-state I-V curves examined for the present study. It is also possible that the differences in discharge regularity are the result of presynaptic mechanisms. Larger, thicker stereocilia and more numerous ribbon synapses are all characteristic of striolar hair cells (Eatock and Songer, 2011) and may contribute to the firing patterns of central dimorphic terminals. Indeed, we found that modulation of hair cell transduction active at rest affects spontaneous firing rate in dimorphic terminals. As discussed in the following sections, modulation of HCN channels in dimorphic terminals also affects regularity of spontaneous firing patterns in vestibular afferent fibers.

Developmental considerations

Data from vestibular ganglion cell bodies were recorded between P0 and P6. Unfortunately, whole-cell, tight-seal recording at later stages becomes prohibitive due to myelination of the cell bodies. Nonetheless, the rodent vestibular system is at least partially functional during the first postnatal week, which suggests that our characterization of I_h is physiologically relevant. Afferent terminals are not myelinated; therefore, we opted to examine calyx terminals at later postnatal stages (P8–12), after which mouse vestibular hair cell maturation has begun to stabilize (Rüsch et al., 1998). Whether the biophysical properties of I_h in vestibular ganglion cell bodies and calyx terminals continue to mature at later developmental stages is not clear. However, we note that Lasker et al. (2008) studied firing patterns in mouse semicircular canal afferent fibers and reported that spike regularity
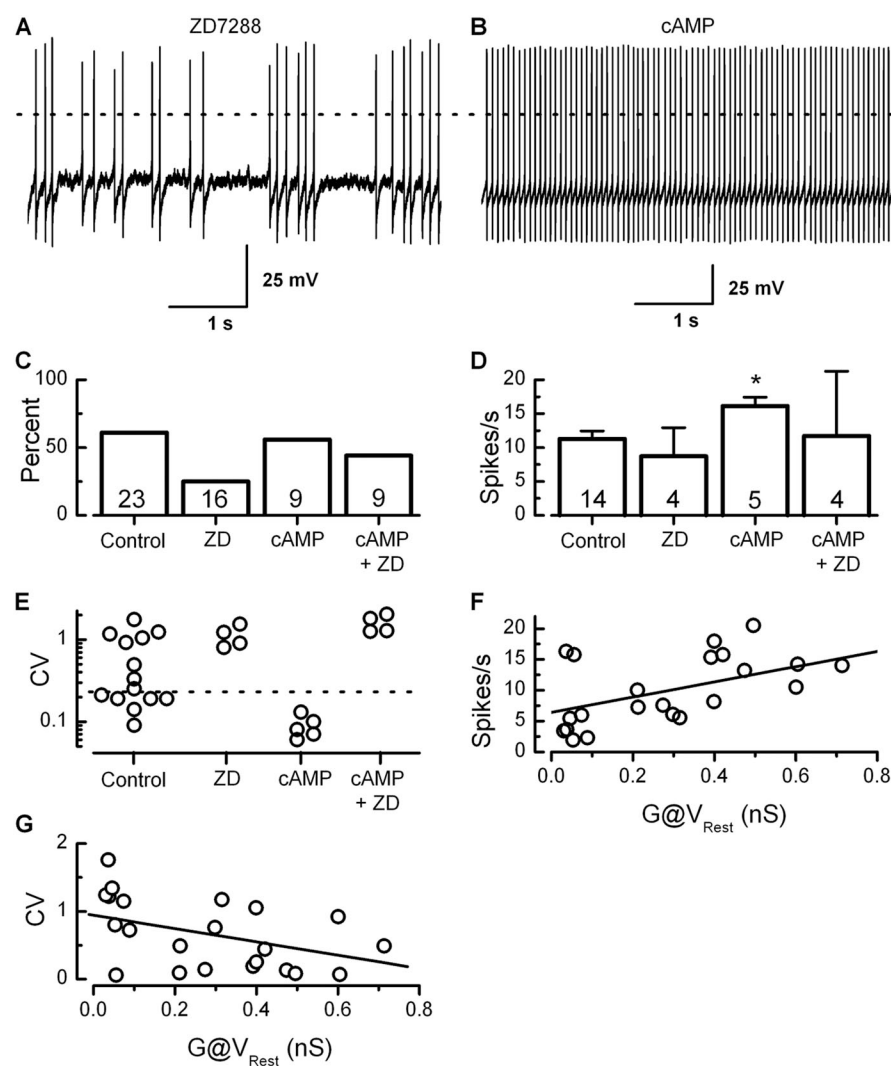

Figure 9. Spontaneous firing rate and regularity are modulated by HCN channel activity. (A and B) Representative traces of spontaneously active calyx terminals in the presence of ZD7288 or cAMP, respectively. The broken line indicates 0 mV. (C) The percentage of calyx terminals that fired spontaneous action potentials. The number of terminals is indicated for each condition. Note that inhibition of I_h resulted in fewer spontaneously active calyx terminals. (D) The mean spike rate plotted for four conditions revealed that cAMP increased the mean rate. *, $P < 0.05$. The number of samples is shown inside the bars for each condition. Error bars indicate mean ± SEM. (E) Wild-type, control calyx terminals fired either regularly or irregularly. The broken line indicates a CV of 0.25. Inhibition of I_h with ZD7288 resulted in irregular firing, whereas cAMP resulted in only regular firing. This cAMP effect was the result of modulation of I_h, as it could be blocked by ZD7288. (F) A plot of G_h at rest versus spike rate shows a positive correlation. The linear fit indicates a statistically significant correlation ($P < 0.01$). (G) A plot of G_h at rest versus CV shows a similar statistically significant correlation ($P < 0.05$).

continued to mature beyond 4 wk of age, with a greater percentage of irregular fibers at later stages. Firing rates were higher than those reported here, perhaps due to developmental changes. Alternatively, the difference in firing rate may be caused by the location of the recording and the recording technique. While we recorded spike activity in calyx terminals using whole-cell electrodes, Lasker et al. (2008) recorded from vestibular nerve fibers using extracellular electrodes. The later technique was used to detect activity in fibers that were spontaneously active and included the summed spike activity that may have originated from multiple synaptic terminals, whereas our data, recorded from single calyx terminals, were unbiased by the pattern of spontaneous activity. As such, caution is warranted when comparing data acquired using different techniques, preparations, organs, species, and developmental stages.

HCN channel composition depends on location

We show that I_h in dimorphic terminals has twice the amplitude of I_h in cell bodies. Furthermore, we find that the molecular composition of the channels that carry I_h differs depending on location. I_h in dimorphic calyx terminals is completely absent in *Hcn1/2*-deficient mice, while small I_h in the cell bodies remains. This implicates a combination of HCN1 and -2 in calyx terminals and HCN1, -2, and perhaps -4 in the cell bodies. These conclusions are supported by our localization data that

showed HCN1 and -2 subunits in the sensory epithelium (Horwitz et al., 2011) and HCN1, -2, and -4 subunits in the cell bodies. Given the prominence of *Hcn2* expression, we found it surprising that there was not a significant decrease in conductance in *Hcn2*-deficient cell bodies. Because *Hcn2* is highly expressed, we speculate that *Hcn1* and *Hcn4* may be up-regulated to compensate for loss of *Hcn2*. If so, this could result in stable conductance levels but different subunit-dependent properties, like activation range and kinetics. Indeed, we found that *Hcn2*-deficient neurons had faster activation kinetics and a small positive shift of the voltage dependence, which is consistent with a greater contribution from HCN1 subunits in the *Hcn2*-deficient neurons. However, HCN4 subunits activate at more negative voltages and with slower kinetics, which suggests that any up-regulation of *Hcn4* expression in the *Hcn2* mutants is minimal. In the absence of electrophysiology data from *Hcn4*-deficient mice, the suggestion that HCN4 may play a role in vestibular neuron cell bodies relies heavily on the immunolocalization and qPCR data.

Deletion of *Hcn2* resulted in an ∼33% reduction in the number of dimorphic terminals with I_h, which suggests that HCN2 subunits play a more prominent role in dimorphic terminals than in cell bodies. Previous studies have shown high levels of HCN channels targeted to dendritic terminals in other neuronal systems (Magee 1999; Narayanan and Johnston 2007; Endo et al., 2008);
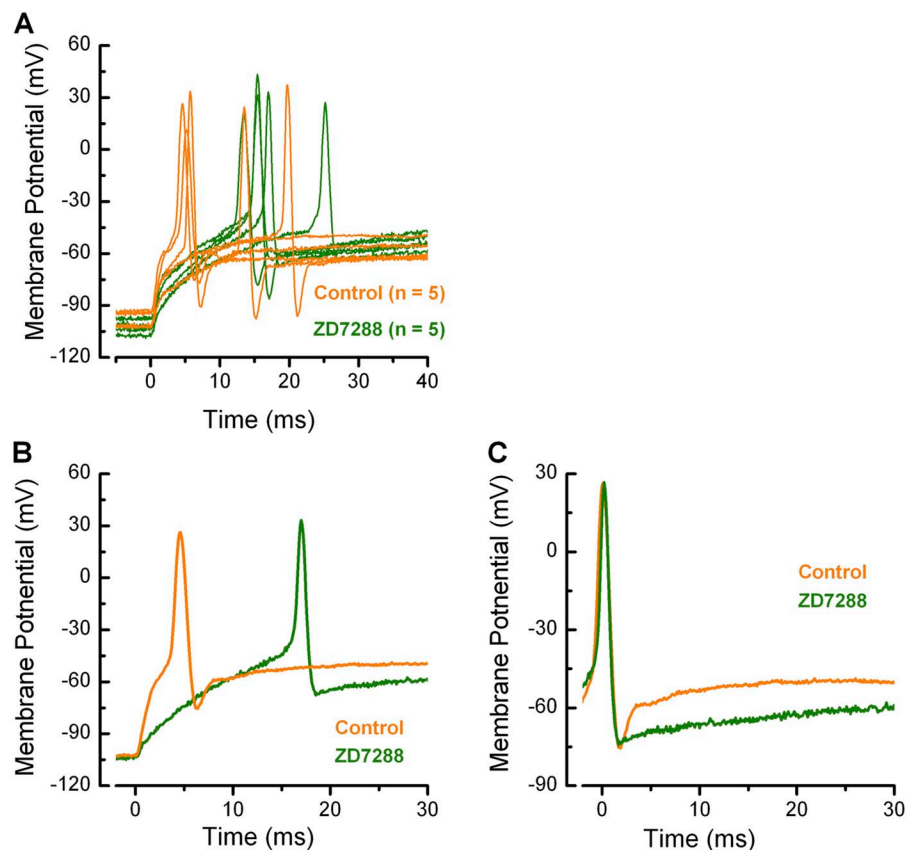
Figure 10. Effects of ZD7288 on calyx action potentials. Traces for control (orange, *n* = 5) and ZD7288-treated (green, *n* = 5) calyx terminals. Action potentials were generated by injecting a hyperpolarizing current sufficient to hold the membrane potential near −100 mV for 300 ms and then stepping back to the zero current level. In each case, a rebound action potential fired without additional current injection. (A) In control cells, action potentials occurred with shorter latencies, whereas in the presence of ZD7288 the latencies were longer. There was no difference in amplitude, which confirms that there is no effect of ZD7288 on Na⁺ channels. During the afterhyperpolarization (AHP), control calyx terminals reached hyperpolarized potentials and then quickly returned to rest. In ZD7288-treated calyx terminals, the AHP was very slow to return to rest. (B) Two representative traces from A are shown on an expanded time scale. Note the long latency of the action potential in the presence of ZD7288. (C) The traces shown in B were aligned at their peaks to highlight differences in the AHP. Note that the ZD7288-treated calyx terminal took longer to return to rest.

however, our data are the first to demonstrate differential distribution of HCN subunits to different regions within the same population of neurons. We hypothesize that HCN2 is the most prominent subunit in dimorphic terminals due to its greater cyclic nucleotide sensitivity, relative to HCN1, which makes it better suited for modulation by cAMP and perhaps modulation by efferent feedback mechanisms (Boyle et al., 2009).

Mechanotransduction contributes to the vestibular afferent spike rate

Spontaneous afferent spiking in lateral-line neurons has previously been shown to depend on hair cell neurotransmission in zebrafish (Trapani and Nicolson, 2011). Here, we extend those observations and present evidence for a similar mechanism in the mammalian vestibular system. We found that hair cell transduction active at rest affects both the number of spontaneously active calyx terminals and the spontaneous firing rate. Deflection of single hair bundles in the positive direction increased firing above the spontaneous rate. Negative bundle deflections decreased the spontaneous rate, confirming that resting mechanotransduction contributes to spontaneous activity in dimorphic terminals. However, negative deflection of single hair bundles did not eliminate firing completely. Therefore, we wondered whether resting activity in neighboring hair bundles, connected postsynaptically through an entire terminal field, may have contributed to the activity that remained. After eliminating mechanotransduction in the entire utricle epithelium by breaking tip links with EGTA, we found that spontaneous activity remained in 44% of dimorphic terminals, which suggests that the remaining activity may arise from other sources, perhaps postsynaptically.

HCN channels contribute to spike regularity

Previous work suggested that spike regularity is partially determined by electrical properties intrinsic to the afferent neurons (Goldberg et al., 1984; Kalluri et al., 2010). Thus, we wondered whether HCN channels in dimorphic terminals may contribute to spontaneous activity. In other neuronal systems, HCN channels have been shown to facilitate initiation of spontaneous action potentials in both neuronal cell bodies (Chan et al., 2011) and dendritic terminals (Endo et al., 2008). Combinations of HCN1 and HCN2 in particular have been shown to determine firing regularity in globus pallidus neurons (Chan et al., 2004). In auditory neurons, HCN channels have been shown to modulate postsynaptic responses (Yi et al., 2010) and contribute to spike timing (Kim and Holt, 2013). Here we report that I_h, carried by HCN1 and HCN2, contributes to spontaneous activity and spike regularity in mouse vestibular ganglion neurons. Firing rate and regularity were positively correlated with G_h half-activation voltage and even more strongly with G_h active at rest.

HCN channels in calyx terminals likely modulate firing activity by passing depolarizing current at hyperpolarized membrane potentials. As a result of their mixed cationic selectivity, the reversal potential for HCN channels is near -40 mV. I_h therefore provides a depolarizing current at potentials negative to -40 mV, helping to drive the membrane toward the threshold for spike initiation. Because the activation/deactivation kinetics of HCN channels are slow relative to the speed of an action potential, their open probability is not significantly altered during the 1–2-ms action potential duration. Rather, tonic I_h active at rest provides a small but continuous depolarizing influence during the interspike interval. At the end of a spike, I_h facilitates faster repolarization during the afterhyperpolarization phase of the action potential and speeds the membrane time constant by decreasing input resistance. Our data suggest that the tonic depolarizing influence of I_h can contribute to spontaneous activity in dimorphic terminals. As we showed that cAMP shifts the voltage dependence of G_h in the positive direction, I_h active at rest is larger and the depolarizing influence of I_h is enhanced. Indeed, we showed that intracellular elevation of cAMP levels increased both the spike rate and regularity in dimorphic terminals. This effect was blocked by ZD7288, which confirms that the cAMP effect was specific to HCN channels. Whether endogenous cAMP levels are elevated in peripheral dimorphic terminals with regular firing patterns relative to levels in central dimorphic terminals that fire irregularly remains to be determined. Regardless, modulation of cAMP levels by endogenous mechanisms or by efferent feedback seems to be a plausible mechanism for regulation of spontaneous activity in vestibular afferent fibers.

REFERENCES

Almanza, A., E. Luis, F. Mercado, R. Vega, and E. Soto. 2012. Molecular identity, ontogeny, and cAMP modulation of the hyperpolarization-activated current in vestibular ganglion neurons. *J. Neurophysiol.* 108:2264–2275. http://dx.doi.org/10.1152/jn.00337.2012

Assad, J.A., G.M. Shepherd, and D.P. Corey. 1991. Tip-link integrity and mechanical transduction in vertebrate hair cells. *Neuron.* 7:985–994. http://dx.doi.org/10.1016/0896-6273(91)90343-X

Baird, R.A., G. Desmadryl, C. Fernández, and J.M. Goldberg. 1988. The vestibular nerve of the chinchilla. II. Relation between afferent response properties and peripheral innervation patterns in the semicircular canals. *J. Neurophysiol.* 60:182–203.

BoSmith, R.E., I. Briggs, and N.C. Sturgess. 1993. Inhibitory actions of ZENECA ZD7288 on whole-cell hyperpolarization activated inward current (If) in guinea-pig dissociated sinoatrial node cells. *Br. J. Pharmacol.* 110:343–349. http://dx.doi.org/10.1111/j.1476-5381.1993.tb13815.x

Boyle, R., R.D. Rabbitt, and S.M. Highstein. 2009. Efferent control of hair cell and afferent responses in the semicircular canals. *J. Neurophysiol.* 102:1513–1525. http://dx.doi.org/10.1152/jn.91367.2008

Chabbert, C., J.M. Chambard, J. Valmier, A. Sans, and G. Desmadryl. 2001. Hyperpolarization-activated (I_h) current in mouse vestibular primary neurons. *Neuroreport.* 12:2701–2704. http://dx.doi.org/10.1097/00001756-200108280-00022

Chambard, J.M., and J.F. Ashmore. 2005. Regulation of the voltage-gated potassium channel KCNQ4 in the auditory pathway. *Pflugers Arch.* 450:34–44. http://dx.doi.org/10.1007/s00424-004-1366-2

Chan, C.S., R. Shigemoto, J.N. Mercer, and D.J. Surmeier. 2004. HCN2 and HCN1 channels govern the regularity of autonomous pacemaking and synaptic resetting in globus pallidus neurons. *J. Neurosci.* 24:9921–9932. http://dx.doi.org/10.1523/JNEUROSCI.2162-04.2004

Chan, C.S., K.E. Glajch, T.S. Gertler, J.N. Guzman, J.N. Mercer, A.S. Lewis, A.B. Goldberg, T. Tkatch, R. Shigemoto, S.M. Fleming, et al. 2011. HCN channelopathy in external globus pallidus neurons in models of Parkinson's disease. *Nat. Neurosci.* 14:85–92. http://dx.doi.org/10.1038/nn.2692

Dhawan, R., S.E. Mann, F.L. Meredith, and K.J. Rennie. 2010. K$^+$ currents in isolated vestibular afferent calyx terminals. *J. Assoc. Res. Otolaryngol.* 11:463–476. http://dx.doi.org/10.1007/s10162-010-0213-8

Dulon, D., S. Safieddine, S.M. Jones, and C. Petit. 2009. Otoferlin is critical for a highly sensitive and linear calcium-dependent exocytosis at vestibular hair cell ribbon synapses. *J. Neurosci.* 29:10474–10487. http://dx.doi.org/10.1523/JNEUROSCI.1009-09.2009

Eatock, R.A., and J.E. Songer. 2011. Vestibular hair cells and afferents: two channels for head motion signals. *Annu. Rev. Neurosci.* 34:501–534. http://dx.doi.org/10.1146/annurev-neuro-061010-113710

Endo, T., E. Tarusawa, T. Notomi, K. Kaneda, M. Hirabayashi, R. Shigemoto, and T. Isa. 2008. Dendritic I_h ensures high-fidelity dendritic spike responses of motion-sensitive neurons in rat superior colliculus. *J. Neurophysiol.* 99:2066–2076. http://dx.doi.org/10.1152/jn.00556.2007

Géléoc, G.S., J.R. Risner, and J.R. Holt. 2004. Developmental acquisition of voltage-dependent conductances and sensory signaling in hair cells of the embryonic mouse inner ear. *J. Neurosci.* 24:11148–11159. http://dx.doi.org/10.1523/JNEUROSCI.2662-04.2004

Goldberg, J.M. 2000. Afferent diversity and the organization of central vestibular pathways. *Exp. Brain Res.* 130:277–297. http://dx.doi.org/10.1007/s002210050033

Goldberg, J.M., and C. Fernández. 1977. Conduction times and background discharge of vestibular afferents. *Brain Res.* 122:545–550. http://dx.doi.org/10.1016/0006-8993(77)90465-6

Goldberg, J.M., C.E. Smith, and C. Fernández. 1984. Relation between discharge regularity and responses to externally applied galvanic currents in vestibular nerve afferents of the squirrel monkey. *J. Neurophysiol.* 51:1236–1256.

Goldberg, J.M., G. Desmadryl, R.A. Baird, and C. Fernández. 1990. The vestibular nerve of the chinchilla. IV. Discharge properties of utricular afferents. *J. Neurophysiol.* 63:781–790.

Hirvonen, T.P., L.B. Minor, T.E. Hullar, and J.P. Carey. 2005. Effects of Intratympanic Gentamicin on Vestibular Afferents and Hair Cells in the Chinchilla. *J. Neurophysiol.* 93:643–655. http://dx.doi.org/10.1152/jn.00160.2004

Holt, J.R., D.P. Corey, and R.A. Eatock. 1997. Mechanoelectrical transduction and adaptation in hair cells of the mouse utricle, a low-frequency vestibular organ. *J. Neurosci.* 17:8739–8748.

Horwitz, G.C., A. Lelli, G.S. Géléoc, and J.R. Holt. 2010. HCN channels are not required for mechanotransduction in sensory hair cells of the mouse inner ear. *PLoS ONE.* 5:e8627. http://dx.doi.org/10.1371/journal.pone.0008627

Horwitz, G.C., J.R. Risner-Janiczek, S.M. Jones, and J.R. Holt. 2011. HCN channels expressed in the inner ear are necessary for normal balance function. *J. Neurosci.* 31:16814–16825. http://dx.doi.org/10.1523/JNEUROSCI.3064-11.2011

Hudspeth, A.J. 1989. How the ear's works work. *Nature.* 341:397–404. http://dx.doi.org/10.1038/341397a0

Hurley, K.M., S. Gaboyard, M. Zhong, S.D. Price, J.R. Wooltorton, A. Lysakowski, and R.A. Eatock. 2006. M-like K+ currents in type I hair cells and calyx afferent endings of the developing rat utricle. *J. Neurosci.* 26:10253–10269. http://dx.doi.org/10.1523/JNEUROSCI.2596-06.2006

Jagger, D.J., and J.F. Ashmore. 1999. The fast activating potassium current, $I_{K,f}$, in guinea-pig inner hair cells is regulated by protein kinase A. *Neurosci. Lett.* 263:145–148. http://dx.doi.org/10.1016/S0304-3940(99)00128-7

Kalluri, R., J. Xue, and R.A. Eatock. 2010. Ion channels set spike timing regularity of mammalian vestibular afferent neurons. *J. Neurophysiol.* 104:2034–2051. http://dx.doi.org/10.1152/jn.00396.2010

Kim, Y.H., and J.R. Holt. 2013. Functional contributions of HCN channels in the primary auditory neurons of the mouse inner ear. *J. Gen. Physiol.* 142:207–223. http://dx.doi.org/10.1085/jgp.201311019

Lasker, D.M., G.C. Han, H.J. Park, and L.B. Minor. 2008. Rotational responses of vestibular-nerve afferents innervating the semicircular canals in the C57BL/6 mouse. *J. Assoc. Res. Otolaryngol.* 9:334–348. http://dx.doi.org/10.1007/s10162-008-0120-4

Lelli, A., P. Kazmierczak, Y. Kawashima, U. Müller, and J.R. Holt. 2010. Development and regeneration of sensory transduction in auditory hair cells requires functional interaction between cadherin-23 and protocadherin-15. *J. Neurosci.* 30:11259–11269. http://dx.doi.org/10.1523/JNEUROSCI.1949-10.2010

Levin, M.E., and J.R. Holt. 2012. The function and molecular identity of inward rectifier channels in vestibular hair cells of the mouse inner ear. *J. Neurophysiol.* 108:175–186. http://dx.doi.org/10.1152/jn.00098.2012

Lim, R., A.E. Kindig, S.W. Donne, R.J. Callister, and A.M. Brichta. 2011. Potassium accumulation between type I hair cells and calyx terminals in mouse crista. *Exp. Brain Res.* 210:607–621. http://dx.doi.org/10.1007/s00221-011-2592-4

Ludwig, A., X. Zong, J. Stieber, R. Hullin, F. Hofmann, and M. Biel. 1999. Two pacemaker channels from human heart with profoundly different activation kinetics. *EMBO J.* 18:2323–2329. http://dx.doi.org/10.1093/emboj/18.9.2323

Ludwig, A., T. Budde, J. Stieber, S. Moosmang, C. Wahl, K. Holthoff, A. Langebartels, C. Wotjak, T. Munsch, X. Zong, et al. 2003. Absence epilepsy and sinus dysrhythmia in mice lacking the pacemaker channel HCN2. *EMBO J.* 22:216–224. http://dx.doi.org/10.1093/emboj/cdg032

Lysakowski, A., S. Gaboyard-Niay, I. Calin-Jageman, S. Chatlani, S.D. Price, and R.A. Eatock. 2011. Molecular microdomains in a sensory terminal, the vestibular calyx ending. *J. Neurosci.* 31:10101–10114. http://dx.doi.org/10.1523/JNEUROSCI.0521-11.2011

Magee, J.C. 1999. Dendritic I_h normalizes temporal summation in hippocampal CA1 neurons. *Nat. Neurosci.* 2:508–514. http://dx.doi.org/10.1038/9158

Marquis, R.E., and A.J. Hudspeth. 1997. Effects of extracellular Ca^{2+} concentration on hair-bundle stiffness and gating-spring integrity in hair cells. *Proc. Natl. Acad. Sci. USA.* 94:11923–11928. http://dx.doi.org/10.1073/pnas.94.22.11923

Meredith, F.L., T.A. Benke, and K.J. Rennie. 2012. Hyperpolarization-activated current (I_h) in vestibular calyx terminals: characterization and role in shaping postsynaptic events. *J. Assoc. Res. Otolaryngol.* 13:745–758. http://dx.doi.org/10.1007/s10162-012-0342-3

Narayanan, R., and D. Johnston. 2007. Long-term potentiation in rat hippocampal neurons is accompanied by spatially widespread changes in intrinsic oscillatory dynamics and excitability. *Neuron.* 56:1061–1075. http://dx.doi.org/10.1016/j.neuron.2007.10.033

Nolan, M.F., G. Malleret, K.H. Lee, E. Gibbs, J.T. Dudman, B. Santoro, D. Yin, R.F. Thompson, S.A. Siegelbaum, E.R. Kandel, and A. Morozov. 2003. The hyperpolarization-activated HCN1 channel is important for motor learning and neuronal integration by cerebellar Purkinje cells. *Cell.* 115:551–564. http://dx.doi.org/10.1016/S0092-8674(03)00884-5

Pattnaik, B.R., and B.A. Hughes. 2012. Effects of KCNQ channel modulators on the M-type potassium current in primate retinal pigment epithelium. *Am. J. Physiol. Cell Physiol.* 302:C821–C833. http://dx.doi.org/10.1152/ajpcell.00269.2011

Rennie, K.J., and M.A. Streeter. 2006. Voltage-Dependent Currents in Isolated Vestibular Afferent Calyx Terminals. *J. Neurophysiol.* 95:26–32. http://dx.doi.org/10.1152/jn.00641.2005

Risner, J.R., and J.R. Holt. 2006. Heterogeneous potassium conductances contribute to the diverse firing properties of postnatal mouse vestibular ganglion neurons. *J. Neurophysiol.* 96:2364–2376. http://dx.doi.org/10.1152/jn.00523.2006

Rüsch, A., A. Lysakowski, and R.A. Eatock. 1998. Postnatal development of type I and type II hair cells in the mouse utricle: acquisition of voltage-gated conductances and differentiated morphology. *J. Neurosci.* 18:7487–7501.

Santoro, B., S. Chen, A. Luthi, P. Pavlidis, G.P. Shumyatsky, G.R. Tibbs, and S.A. Siegelbaum. 2000. Molecular and functional heterogeneity of hyperpolarization-activated pacemaker channels in the mouse CNS. *J. Neurosci.* 20:5264–5275.

Songer, J.E., and R.A. Eatock. 2013. Tuning and timing in mammalian type I hair cells and calyceal synapses. *J. Neurosci.* 33:3706–3724. http://dx.doi.org/10.1523/JNEUROSCI.4067-12.2013

Sousa, A.D., L.R. Andrade, F.T. Salles, A.M. Pillai, E.D. Buttermore, M.A. Bhat, and B. Kachar. 2009. The septate junction protein caspr is required for structural support and retention of KCNQ4 at calyceal synapses of vestibular hair cells. *J. Neurosci.* 29:3103–3108. http://dx.doi.org/10.1523/JNEUROSCI.4868-08.2009

Trapani, J.G., and T. Nicolson. 2011. Mechanism of spontaneous activity in afferent neurons of the zebrafish lateral-line organ. *J. Neurosci.* 31:1614–1623. http://dx.doi.org/10.1523/JNEUROSCI.3369-10.2011

Wu, X., L. Liao, X. Liu, F. Luo, T. Yang, and C. Li. 2012. Is ZD7288 a selective blocker of hyperpolarization-activated cyclic nucleotide-gated channel currents? *Channels (Austin).* 6:438–442. http://dx.doi.org/10.4161/chan.22209

Yi, E., I. Roux, and E. Glowatzki. 2010. Dendritic HCN channels shape excitatory postsynaptic potentials at the inner hair cell afferent synapse in the mammalian cochlea. *J. Neurophysiol.* 103:2532–2543. http://dx.doi.org/10.1152/jn.00506.2009